



# Photometric and Spectroscopic Studies for Two Magnetic-activity Contact Binaries: V724 And and QR Com

Shuang Wang<sup>1</sup>, Raúl Meichel<sup>2</sup> , Huiyu Yuan<sup>1</sup> , and Yuangui Yang<sup>1,3</sup> 

<sup>1</sup> School of Physics and Electronic Information, Huaibei Normal University, Huaibei City 235000, China; [yygcn@163.com](mailto:yygcn@163.com)

<sup>2</sup> Observatorio Astronómico Nacional, Instituto de Astronomía, Universidad Nacional Autónoma de México, Apartado Postal 877, Ensenada, B.C. 22830, México  
Received 2022 July 12; accepted 2022 August 4; published 2022 October 12

## Abstract

We presented new CCD photometry for two contact binaries, V724 And and QR Com, which were observed during the 2020–2022 observing seasons. By using the Wilson–Devinney method, the photometric solutions were deduced from new observed data and TESS ones. Their asymmetric light curves were modeled by a dark spot on the more massive component. Results indicate that the starspot may immigrate or disappear on the surface of the active component. From the TESS observations of QR Com, it is discovered that the difference between light maxima exhibits a 29.5 day oscillation, which implies the continuous evolution of spot feathers on the timescale of several weeks. Their mass ratio and fill-out factor are  $q = 2.308$  and  $f = 11.55\%$  for V724 And, and  $q = 0.624$  and  $f = 12.77\%$  for QR Com, respectively. From the ( $O-C$ ) curve, the orbital period secularly decrease at a rate of  $dP/dt = -1.66 \times 10^{-7} \text{ day yr}^{-1}$  for V724 And and  $dP/dt = -3.98 \times 10^{-7} \text{ day yr}^{-1}$  for QR Com, which was interpreted by mass transfer from the more massive component to the less massive one. With period decreasing, this kind of shallow-contact binaries, V724 And and QR Com, will evolve into the deep-contact configurations.

*Key words:* (stars:) binaries: eclipsing – stars: fundamental parameters – stars: low-mass

## 1. Introduction

W UMa-type stars are late-type contact binaries with a common convective envelope (Lucy 1968), whose components fill their Roche lobes. The spectral types range from F to K with a typical period of around 0.4 days. Their progenitors may evolve into contact configurations by angular momentum loss from magnetic breaking (Stępień 2011), which are undergoing a process of thermal relaxation oscillation, i.e., TRO theory (Webbink 2003). Some complicated physical processes and special phenomena in contact binaries have been attracted by many investigators, such as Qian et al. (2017), Chen et al. (2020), Gazeas et al. (2021) and Loukaidou et al. (2022). Recently, Latković et al. (2021) have studied  $\sim 700$  well-observed contact binaries and obtained some key statistical relation between the parameters of binaries. The late-type contact binaries usually show strong magnetic activity including starspots (Pi et al. 2019; Yang et al. 2022), flares (Qian et al. 2014; Huang et al. 2020) and chromospheric activity (Whelan et al. 2021). The light curves exhibit an unheight between both light maxima, i.e., O’Connell (1951) effect. In present paper, we chose two neglected contact binaries, V724 And and QR Com as our observed targets, in order to study the immigration and evolution of their starspots.

QR Com (=BD+22 2561, 1RXS J131501.3+211356) is an EW-type eclipsing binary with a period of 0.427 864 days (Samus et al. 2017). Its visual magnitude varies from  $8^m.93$  to

$9^m.19$ . Kiraga (2012) classified its spectral type to be G2, which was revised to be F5/6 by the LAMOST survey spectra.<sup>4</sup> From the Gaia DR2 database,<sup>5</sup> QR Com is considered a single star with an effective temperature of 6343 K, radius of  $1.65 R_{\odot}$  and luminosity of  $3.987 L_{\odot}$  (Gaia Collaboration et al. 2018). Zichgraf et al. (2003) listed it as one of the ROSAT bright source catalog X-ray sources. Therefore, QR Com may have the starspot activity. Another eclipsing binary V724 And (=ASAS J003244+2506.8) has a short period of 0.268 176 days (Drake et al. 2014). Its visual magnitude ranges from  $13^m.08$  to  $13^m.68$ . Its temperature, radius and luminosity are 5114 K,  $0.97 R_{\odot}$  and  $0.584 L_{\odot}$  from the Gaia DR2 database. From LAMOST spectral database, V724 And processed a spectral type of G7/8. Except TESS survey observations,<sup>6</sup> no light curves and period analysis for two binaries have been published up to now.

## 2. Photometric and Spectroscopic Observations

### 2.1. New Photometry

New photometry for V724 And was performed from 2020 December to 2021 November by using the 60 cm telescope at the Xinglong station (XLS) of National Astronomical Observatories, Chinese Academy of Sciences (NAOC). For QR Com, Dr. Meichel observed this binary by the 84 cm telescope at the

<sup>3</sup> Corresponding author.

<sup>4</sup> <http://dr7.lamost.org>

<sup>5</sup> <https://cdsarc.cds.unistra.fr/viz-bin/cat/I/345>

<sup>6</sup> <https://mast.stsci.edu/portal/Mashup/Clients/Mast/Portal.html>

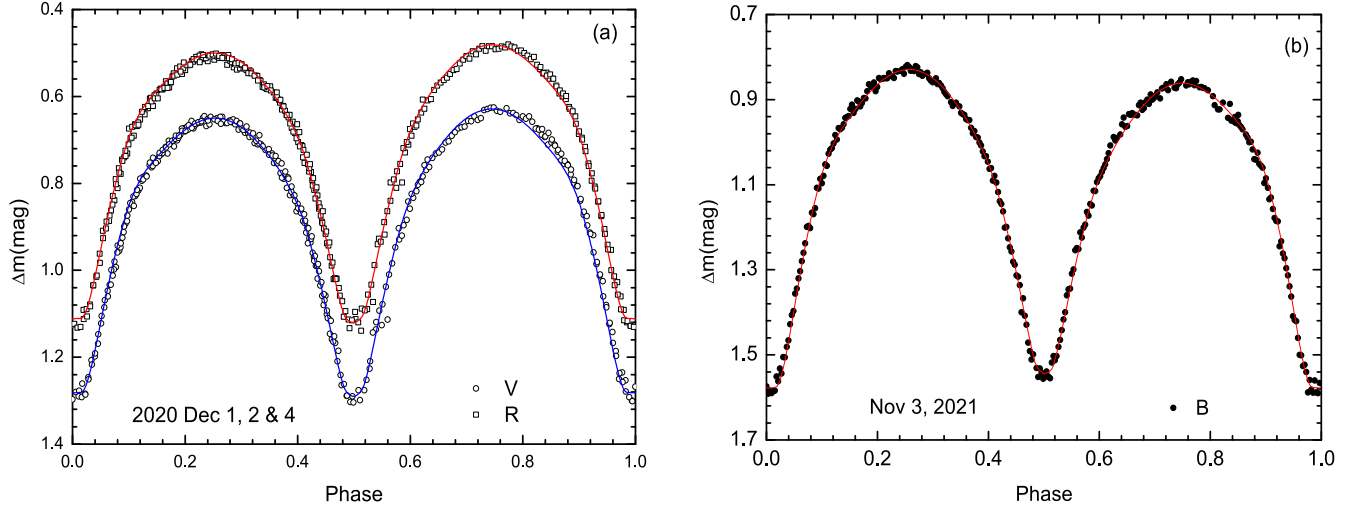


**Figure 1.** New observations for V724 And, which were obtained in 2020 (a) and 2021 (b). Theoretical LCs as color lines are constructed by the solutions from Table 3.

National Astronomical Observatory of Mexico on 2022 May 19 and 20. The standard *UBVRcIc* filters were employed on both telescopes. In observing data reductions, IRAF software was used including bias, flat field and aperture photometry. All individual observations were available on request.

For V724 And, we chose the comparison star ( $\alpha_{J2000.0} = 00^{\text{h}}32^{\text{m}}41^{\text{s}}.93$  and  $\delta_{J2000.0} = +24^{\circ}00'29''$ ) and check star ( $\alpha_{J2000.0} = 00^{\text{h}}32^{\text{m}}33^{\text{s}}.36$  and  $\delta_{J2000.0} = +25^{\circ}09'29''$ ). The typical exposure times are 50 s and 60 s for *VRc* observations, respectively. The complete light curves in 2000 (i.e.,  $LC_{2000}$ ) and *B* band LC (i.e.,  $LC_{2021}$ ) are displayed in both panels of Figure 1, whose phases are computed by the period of  $0^{\text{d}}.268177$  (Dithelm 2011). For another binary QR Com, we adopted the comparison star ( $\alpha_{J2000.0} = 13^{\text{h}}14^{\text{m}}39^{\text{s}}.64$  and  $\delta_{J2000.0} = +21^{\circ}12'24''$ ) and check star ( $\alpha_{J2000.0} = 13^{\text{h}}14^{\text{m}}33^{\text{s}}.89$  and  $\delta_{J2000.0} = +21^{\circ}13'47.2''$ ). Exposure times are 9 s, 6 s and 3 s for *BVRc* filters, respectively. The complete light curves are displayed in Figure 2, whose phases are computed by the period of  $0^{\text{d}}.427869$  from the *o-c* gateway.<sup>7</sup>

From Figures 1 and 2, there exists a small unheight between both light maxima for two binaries. In order to qualify this kind of effect, the characteristics of light curves are listed in Table 1, including Max.I–Max.II, the variable amplitude (i.e., Min.I–Max.I), and Min.I–Min.II. This kind of phenomenon (i.e., O’Connell effect) occurs in other contact binaries such as V0576 Peg and KW Psc (Yang et al. 2022), AQ Psc and V384 Ser (Liyun et al. 2021), and CC Com (Zhu et al. 2021), which may be attributed to magnetic activity for late-type binaries.

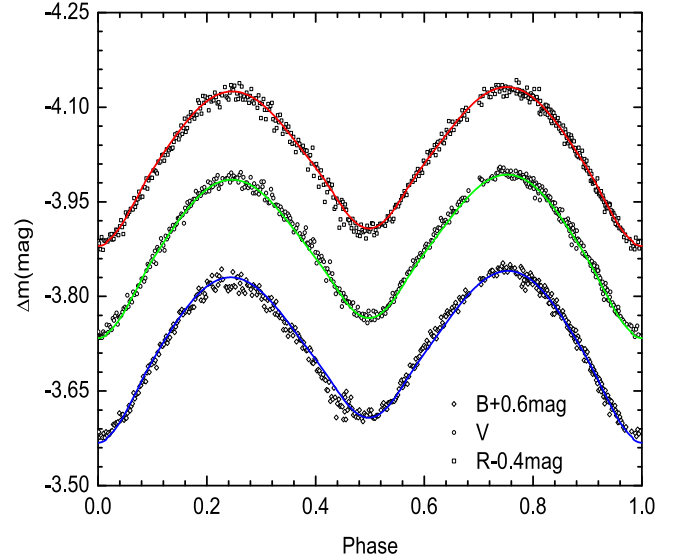


**Figure 2.** *BVR* light curves for QR Com, which were observed by the 84 cm telescope at the National Astronomical Observatory of Mexico on 2021 May 19 and 20.

## 2.2. TESS Observations

From TESS survey data, we obtained a total of 640 observations with an exposure of 30 minutes from 2019 October 7 to November 1. The folded light curve is displayed in Figure 3(a). From this figure, there exists an O’Connell effect, i.e.,  $\text{Max.I} - \text{Max.II} = 0^{\text{m}}.033$ . The light variable amplitude is  $0^{\text{m}}.573$ . For QR Com, we downloaded 16,609 data with the exposure time of 120 seconds from 2020 March 20 to April 15. After normalizing the SAP-FLUX, we obtained the different magnitudes versus BJD times. From these data, we

<sup>7</sup> <http://var2.astro.cz/ocgate/>

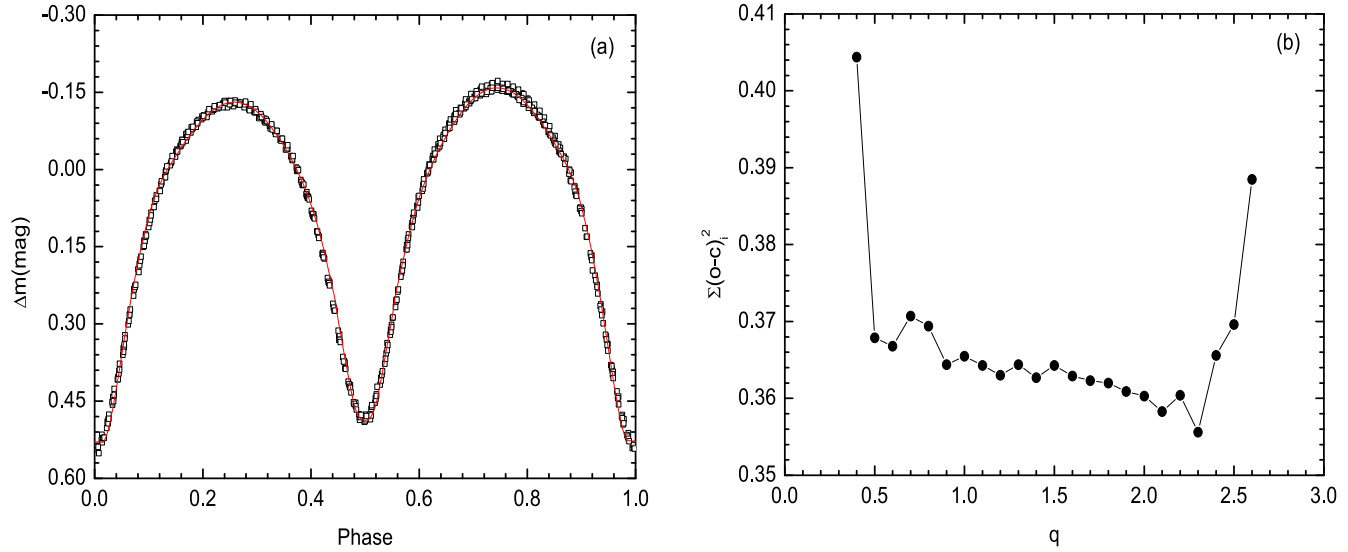


**Figure 3.** (a) TESS light curves for V724 And and theoretical values from the spotted solution. (b) A searching process of mass ratio for V724 And, which was deduced from light curves in 2020.

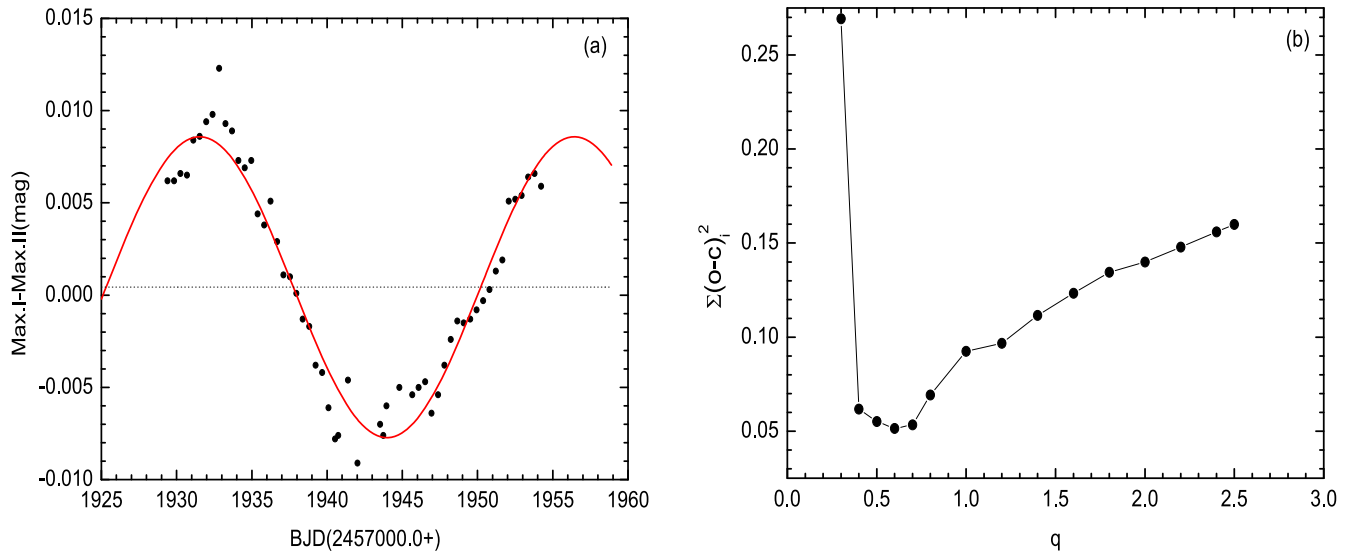


**Figure 4.** (a) The variable of  $Max.I - Max.II$  from TESS continuous data for QR Com. (b) Searching a reliable mass ratio from TIC<sub>1937</sub>.

**Table 1**  
Photometric Characteristics of Light Curves

Variable Star	V724 And		QR Com
	LC <sub>2020</sub>	LC <sub>2021</sub>	
Observing dates	Dec 1, 2, 4, 2020 & Jan 11, 2021	Nov 3, 2021	Feb 1, 2021
Number of data	354 (V) & 363 ( $R_c$ )	310 (B)	499 (B), 504 (V) & 511 ( $R_c$ )
Standard error	0.015 (V) & 0.013 ( $R_c$ )	0.012 (B)	0.009 (B), 0.007 (V) & 0.008 ( $R_c$ )
Min.I-Max.I	0 <sup>m</sup> .644 (V), 0 <sup>m</sup> .628 ( $R_c$ )	0 <sup>m</sup> .764 (B)	0 <sup>m</sup> .239 (B), 0 <sup>m</sup> .238 (V), 0 <sup>m</sup> .235 ( $R_c$ )
Max.I-Max.II	0 <sup>m</sup> .026 (V), 0 <sup>m</sup> .024 ( $R_c$ )	-0 <sup>m</sup> .030 (B)	0 <sup>m</sup> .018 (B), 0 <sup>m</sup> .009 (V), 0 <sup>m</sup> .007 ( $R_c$ )
Min.I-Min.II	-0 <sup>m</sup> .002 (V), -0 <sup>m</sup> .001 ( $R_c$ )	0 <sup>m</sup> .047 (B)	0 <sup>m</sup> .028 (B), 0 <sup>m</sup> .024 (V), 0 <sup>m</sup> .021 ( $R_c$ )

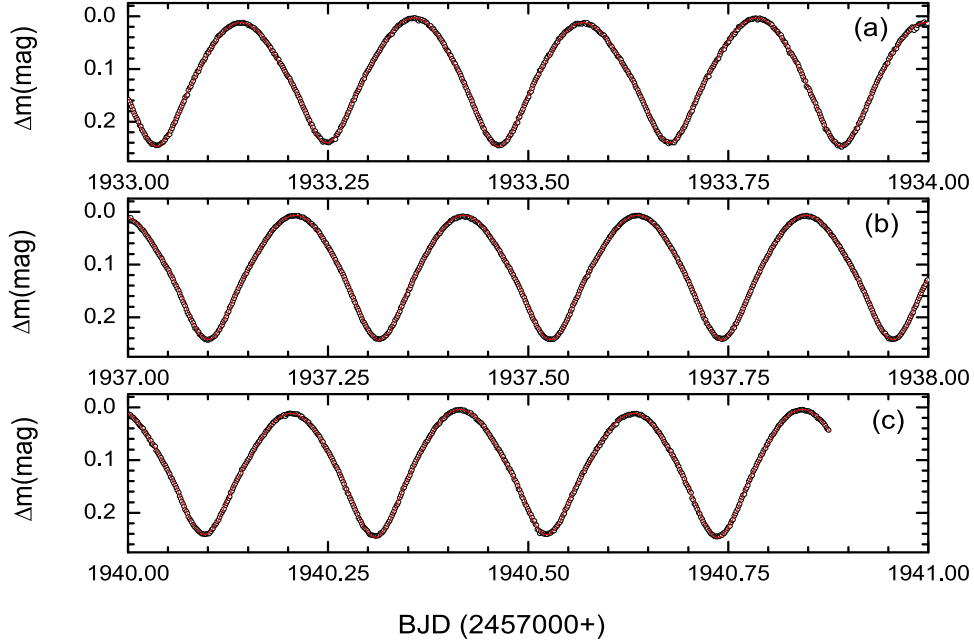


**Figure 5.** Three sets light curves for QR Com, LC<sub>1933</sub> (a), LC<sub>1937</sub> (b) and LC<sub>1940</sub> (c).

found a variable unheight between both light maxima in the 26 days light curves. By using a parabolic fitting method, we obtained the values of maximum light at phase of 0.25 and 0.75, in order to compute the  $\Delta M = \text{Max.I} - \text{Max.II}$  which is displayed in Figure 4(a). From this figure, a cyclic variation seems to occur. Therefore, the values of Max.I–Max.II are fitted a sinusoidal curve as follows,

$$\Delta M = 0^{\text{m}}0004(1) + 0^{\text{m}}0082(6) \times \sin[0.2524(5) \times T_{\text{BJD}} + 4.20(46)], \quad (1)$$

where the parenthesized numbers refer to the standard derivation in units of the last decimal place. From this equation, the modulated period may be  $24.9(\pm 0.5)$  days, which the observed data cover its complete period. This kind of modulated period occurs in other active binaries, such as XY UMa with a period of  $709(\pm 10)$  days (Pribulla et al. 2001). In order to display the intrinsic light variability, we intercepted three segments of light curves (about 1.0 day interval), i.e., TIC<sub>1933</sub>, TIC<sub>1937</sub> and TIC<sub>1940</sub>, which are displayed in Figure 5. The value of  $\Delta M$  varies from  $0^{\text{m}}009$  for TIC<sub>1933</sub> to 0 for TIC<sub>1937</sub>, to  $-0^{\text{m}}007$  for TIC<sub>1940</sub>, which indicates that the cool spot may immigrate or disappear on the active component.

### 2.3. LAMOST Spectra

From LAMOST survey database, we searched four spectra for two binaries, which are listed in Table 2, including observing date, spectral type, temperature and so on. We averaged the temperatures from two spectra and derived the temperature of the more massive component to be 5276

( $\pm 46$ ) K for V724 And, and  $6307(\pm 8)$  K for QR Com, respectively.

For the late-type stars, chromospheric emission lines, such as H $\alpha$  (Soderblom et al. 1993), are the indications of the chromospheric activity. Spectral subtraction technique was widely used to analyze chromosphere activity of stars (Zhang et al. 2020). From LAMOST survey spectra, we chose four standard stars (Huang et al. 2018), whose names, observing dates and temperature are listed in Table 2. The original and subtracted spectra are displayed in Figure 6. From this figure, there evidently exists H $\alpha$  emission line, which implies that V724 And and QR Com may occur magnetic activity.

### 3. Solving Light Curves

For two contact binaries, we adopted mode 3 to deduce the photometric solutions for the light curves by the Wilson-Devinney program (Wilson & Devinney 1971; Wilson & Van Hamme 2014). As usual, some parameters for both components are fixed as bolometric albedo of  $A_{1,2} = 0.5$  (Lucy 1967), gravity darkening coefficients of  $g_{1,2} = 0.32$  (Rucinski 1973), and logarithmic limb darkening coefficients taken from (Van Hamme 1993). Moreover, we set the parameters of  $LD_{1,s} = -2$  for the TESS light curves. Due to no radial velocity curves, a searching process of mass ratios was preformed only from light curves. In solving asymmetric light curves, we assumed the cool spot on the equator of the more massive component (i.e., colatitude  $\theta = 90^\circ$ ). The adjustable parameters are listed as mass ratio  $q$ , inclination  $i$ , dimensionless surface potential  $\Omega_{1,2}$  and  $T_1$  (for A-type) or  $T_2$  (for W-type).

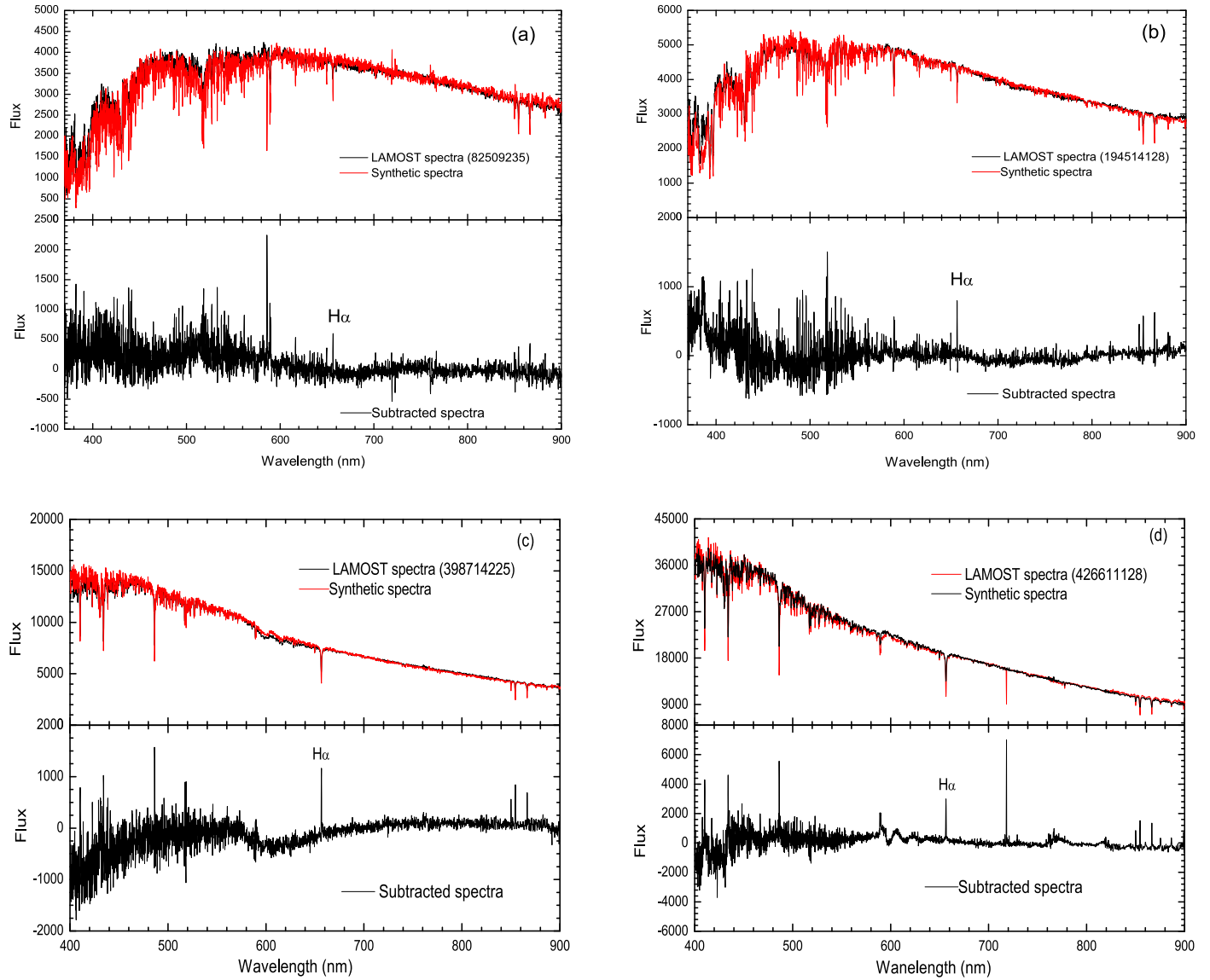


**Figure 6.** The spectra for V724 And (a), (b) and QR Com (c), (d) and their standard stars are taken from the LAMOST survey database.

**Table 2**  
LAMOST Survey Spectra for V724 And and QR Com

Star	V724 And		QR Com	
	sp09-235.fits	sp14-128.fits	sp14-125.fits	sp11-128.fits
Observing dates	Nov 24, 2012	Dec 19, 2013	Dec 25, 2015	Feb 19, 2016
Spectral type	G7	G8	F6	F5
Temperature (K)	$5217 \pm 68$	$5335 \pm 23$	$6307 \pm 8$	$6306 \pm 8$
$\log g$ (dex)	$4.171 \pm 0.112$	$4.387 \pm 0.037$	$4.094 \pm 0.014$	$4.119 \pm 0.012$
Radial velocity ( $\text{kms}^{-1}$ )	$-19.84 \pm 15.06$	$-4.32 \pm 18.26$	$-3.79 \pm 6.18$	$6.73 \pm 6.38$
Standard star	J090555.70+380403.8	J084812.67+121921.8	J061139.19+220218.3	J154117.48+554404.6
Observing dates	Dec 29, 2015	Feb 6, 2016	Dec 19, 2016	Dec 5, 2016
Temperature (K)	$5025 \pm 177$	$5357 \pm 23$	$6255 \pm 30$	$6580 \pm 14$

**Table 3**  
Photometric Solutions and Absolute Parameters for V724 And and QR Com

Parameters	V724 And (W-type)			QR Com (A-type)			
	LC <sub>2020</sub>	LC <sub>2021</sub>	LC <sub>TESS</sub>	TIC <sub>1933</sub>	TIC <sub>1937</sub>	TIC <sub>1940</sub>	LC <sub>2022</sub>
$q = M_2/M_1$	2.308( $\pm 0.004$ )	2.308 <sup>a</sup>	2.308 <sup>a</sup>	0.624 <sup>a</sup>	0.624( $\pm 0.002$ )	0.624 <sup>a</sup>	0.624 <sup>a</sup>
$i(^{\circ})$	84.00( $\pm 0.05$ )	84.35( $\pm 0.18$ )	83.81( $\pm 0.11$ )	58.38( $\pm 0.03$ )	58.08( $\pm 0.02$ )	58.36( $\pm 0.04$ )	58.05( $\pm 0.08$ )
$\Omega_{1,2}$	5.6120 ( $\pm 0.0060$ )	5.6000( $\pm 58$ )	5.5500 ( $\pm 0.0042$ )	3.0655 ( $\pm 0.0005$ )	3.0691 ( $\pm 0.0003$ )	3.0656 ( $\pm 0.0004$ )	3.0605( $\pm 0.0015$ )
$T_1$ (K)	5376( $\pm 0$ )	5457( $\pm 6$ )	5526( $\pm 9$ )			6307( $\pm 8$ ) <sup>a</sup>	
$T_2$ (K)		5276( $\pm 46$ ) <sup>a</sup>		6418( $\pm 8$ )	6347( $\pm 5$ )	6446( $\pm 9$ )	5870( $\pm 17$ )
<sup>b</sup> $\ell_1$ (B)	...	0.3771 ( $\pm 0.0015$ )		...	...	...	0.7004( $\pm 0.0038$ )
$\ell_1$ (V)	0.3415 ( $\pm 0.0014$ )	...	...	...	...	...	0.6772( $\pm 0.0029$ )
$\ell_1$ (Rc)	0.3374 ( $\pm 0.0012$ )	...	...	...	...	...	0.6663( $\pm 0.0025$ )
$\ell_1$ (TESS)	...	...	0.3633 ( $\pm 0.0013$ )	0.6148 ( $\pm 0.0009$ )	0.6068 ( $\pm 0.0006$ )	0.6178(0.0009)	...
<sup>c</sup> $\bar{r}_1$	0.3161 ( $\pm 0.0018$ )	0.3169 ( $\pm 0.0020$ )	0.3230 ( $\pm 0.0021$ )	0.4291 ( $\pm 0.0022$ )	0.4283 ( $\pm 0.0040$ )	0.4291 ( $\pm 0.0028$ )	0.4295( $\pm 0.0028$ )
$\bar{r}_2$	0.4610 ( $\pm 0.0024$ )	0.4622 ( $\pm 0.0028$ )	0.4676 ( $\pm 0.0030$ )	0.3465 ( $\pm 0.0017$ )	0.3455 ( $\pm 0.0030$ )	0.3465 ( $\pm 0.0021$ )	0.3467( $\pm 0.0019$ )
Longitude ( $^{\circ}$ )	77.2( $\pm 0.8$ )	285.3( $\pm 2.8$ )	97.5( $\pm 1.9$ )	103.1( $\pm 0.9$ )	...	277.2( $\pm 2.2$ )	247.2( $\pm 6.5$ )
Spot radius ( $^{\circ}$ )	10.8( $\pm 1.1$ )	11.6( $\pm 1.2$ )	15.4( $\pm 1.3$ )	15.5( $\pm 1.3$ )	...	15.4( $\pm 1.4$ )	9.2( $\pm 1.3$ )
$T_s/T$	0.74( $\pm 0.08$ )	0.85( $\pm 0.09$ )	0.852( $\pm 0.069$ )	0.832( $\pm 0.141$ )	...	0.888 $\pm$ 0.019	0.845( $\pm 0.042$ )
$f$ (%)	11.55( $\pm 0.13$ )	13.54( $\pm 0.13$ )	21.79( $\pm 0.19$ )	11.49( $\pm 0.02$ )	10.47( $\pm 0.01$ )	11.46( $\pm 0.02$ )	12.77( $\pm 0.09$ )
$M_1$ ( $M_{\odot}$ )	0.37( $\pm 0.02$ )						1.36( $\pm 0.04$ ) <sup>a</sup>
$M_2$ ( $M_{\odot}$ )	0.85( $\pm 0.03$ ) <sup>a</sup>						0.85( $\pm 0.03$ )
$a$ ( $R_{\odot}$ )	1.87( $\pm 0.02$ )						3.11( $\pm 0.03$ )
$R_1$ ( $R_{\odot}$ )	0.59( $\pm 0.02$ )						1.34( $\pm 0.05$ )
$R_2$ ( $R_{\odot}$ )	0.86( $\pm 0.03$ )						1.08( $\pm 0.04$ )
$L_1$ ( $L_{\odot}$ )	0.26( $\pm 0.02$ )						2.53( $\pm 0.19$ )
$L_2$ ( $L_{\odot}$ )	0.52( $\pm 0.03$ )						1.24( $\pm 0.09$ )

**Notes.**

<sup>a</sup> Adopted the fixed values.

<sup>b</sup> The relative luminosities can be expressed by  $\ell_{1/2} = L_{1/2}/(L_1 + L_2)$ .

<sup>c</sup> The relative radius is computed by  $\bar{r} = (r_{\text{pole}} + r_{\text{side}} + r_{\text{back}})/3$ .

### 3.1. V724 And

From the contact binary V724 And, three sets of light curves were analyzed to derive photometric solutions. The mean effective temperature of star 2 is adopted to be  $T_2 = 5276(\pm 46)$  K. We first performed a searching process of mass ratios for *VRc* light curves (i. e., LC<sub>2020</sub>). For some a fixed mass ratios ranging from 0.5 to 2.5 with a step of 0.1, we obtained a series of photometric solutions. The resulting  $q - \Sigma$  curve is displayed in Figure 3(b), where a minimum squared residuals  $\Sigma$  is achieved around  $q = 2.3$ . This implies that V724 And is a W-type binary, i.e., star 2 with more massive. Moreover, the maximum light at phase 0.75 from Figure 1(a) is brighter than that at phase 0.25. Therefore, a cool spot is assumed on the surface of star 2. After setting  $q$  and the spot's parameters as free values, we obtained the final photometric solution, which are listed in Table 3. The final mass ratio and

fill-factor for V0724 And are  $q = 2.308(\pm 004)$  and  $f = 11.55(\pm 0.13)\%$ . Theoretical light curves are plotted as continuous lines in Figure 1(a). We accepted this photometric element as the final solution, which was deduced from two-color light curves.

For another sets of light curves, i.e., LC<sub>2021</sub> and LC<sub>TESS</sub>, we fixed a mass ratio of  $q = 2.308$  when deriving the spotted solutions. From Figure 1(b), Max.I is brighter than Max.II up to  $\sim 0^{\text{m}}03$  in LC<sub>2021</sub>. Assumed a cool spot on star 2, we derived another spotted solution, which is listed in Table 3. The spot's area is up to 1.03% of the star 2's surface area. For the LC<sub>TESS</sub> of V724 And, we set the reference epoch in ephemeris,  $t_0$ , as a free parameter in order to determine the primary minimum time. We derived a spotted solution, which is listed in Table 3. The corresponding theoretical light curve is plotted in Figure 3(a).

**Table 4**  
All Available Light Minimum Times for V724 And and QR Com

Stars	JD(Hel.)	Error	Min	Method	Band	References
V724 And	2454408.538	...	Sec	...	...	Dithelm (2011)
	2455511.6846	$\pm 0.0003$	Pri	CCD	V	Dithelm (2011)
	2456256.6788	$\pm 0.0003$	Pri	CCD	V	Diethelm (2013)
	2459185.0241	$\pm 0.0004$	Sec	CCD	V $Rc$	Present study
	2459185.9631	$\pm 0.0002$	Pri	CCD	V $Rc$	Present study
	2459188.1084	$\pm 0.0002$	Pri	CCD	V $Rc$	Present study
	2459209.0261	$\pm 0.0001$	Pri	CCD	V $Rc$	Present study
	2459226.0546	$\pm 0.0002$	Sec	CCD	V $Rc$	Present study
	2459521.9865	$\pm 0.0001$	Pri	CCD	B	Present study
	2459522.1213	$\pm 0.0001$	Sec	CCD	B	Present study
QR Com	2453120.4506	...	Pri	CCD	...	<a href="http://var2.astro.cz/ocgate">http://var2.astro.cz/ocgate</a>
	2454989.386	$\pm 0.010$	Pri	CCD	...	Paschke (2009)
	2457757.693	...	Pri	CCD	...	<a href="http://var2.astro.cz/ocgate">http://var2.astro.cz/ocgate</a>
	2458939.4518	$\pm 0.0017$	Pri	pe	I	Lienhard (2021)
	2458975.3990	$\pm 0.0070$	Pri	CCD	V	Paschke (2020)
	2458988.4475	$\pm 0.0016$	Sec	pe	I	Lienhard (2021)
	2458933.4637	$\pm 0.0002$	Pri	CCD	TESS	Present study
	2458937.3138	$\pm 0.0001$	Pri	CCD	TESS	Present study
	2458940.7364	$\pm 0.0002$	Pri	CCD	TESS	Present study
	2459199.603	$\pm 0.001$	Pri	CCD	V	Paschke (2021)
	2459719.6649	$\pm 0.0006$	Sec	CCD	BV $Rc$	Present study
	2459720.7359	$\pm 0.0003$	Pri	CCD	BV $Rc$	Present study

### 3.2. QR Com

As shown in Figure 4(a), the difference between both light maxima varies with time. There may exist a 25<sup>d</sup>9 periodicity. Max.II from Figure 2 is apparently brighter than Max.I. In order to remove the impact on the reliable mass ratio from the asymmetric light curve, we chose the symmetric light curve, TIC<sub>1937</sub>, to search a mass ratio. Then we derived four sets of photometric elements after inputting the initial mass ratio.

From Table 2, the mean effective temperature for QR Com is adopted to be  $T_1 = 6307(\pm 8)$  K. For 720 TESS observations in TIC<sub>1933</sub>, we performed a “q-search” process and got a  $q - \Sigma$  curve, which is displayed in Figure 4(b). A minimum value of  $\Sigma$  arrived at a mass ratio of  $q = 0.625$ . Therefore, QR Com is an A-type contact binary. After considering  $q = 0.625$  as an input free parameter, we then obtained the final photometric solution, which is listed in Table 3. The mass ratio and fill-out factor of QR Com are  $q = 0.624(\pm 0.002)$  and  $f = 11.47(\pm 0.01)\%$ . For other two sets of TESS light curves (i.e., TIC<sub>1933</sub> and TIC<sub>1940</sub>), a dark spot is assumed on the surface of star 1, meanwhile we fixed a mass ratio of  $q = 0.624$ . We obtained other two sets of spotted solutions, which are also listed in Table 3. Then we computed the corresponding theoretical light curves, which are displayed in Figure 5.

For our new BV $Rc$  light curves, the LC<sub>2022</sub> evidently shows to be asymmetric, in which the value of  $\Delta M$  approximates up to 0<sup>m</sup>.02 in the B band. Assumed a dark spot on the equator of the star 1, we obtained the photometric solution, which is listed

in Table 3. The computed light curves are played as continuous lines in Figure 2. The area of spot is 0.65% of stellar surface. The fill-out factor and orbital inclination are  $f = 12.77(\pm 0.09)\%$  and  $i = 58.05(\pm 0.08)^\circ$ , which implies that QR Com is an A-type partial-eclipsing marginal contact binary. We accepted the final solution for this binary because it was deduced from multi-color light curves. Therefore, it is needed to obtain radial velocities to identify this result.

## 4. Orbital Period Analysis

For the new observations from 2020 to 2022, we determined seven light minimum times by using the method of Kwee & van Woerden (1956). Other eclipsing times of V724 And and Q are taken from the  $o-c$  gateway. Table 4 lists all available times of minimum light, which are used to analyze the orbital period variations for two binaries.

### 4.1. V724 And

Dithelm (2011) gave a preliminary ephemeris with an initial epoch time of 2 454 408.538. However, it is a secondary time of minimum light. From 10 eclipsing times, we updated a linear ephemeris as follows,

$$\text{Min.I} = \text{HJD } 245408.6750(11) + 0.26817603(7) \times E \quad (2)$$

With the help of Equation (2), we computed the initial residuals,  $(O-C)_i$ , which are displayed in the upper panel of Figure 7(a). From this figure, the orbital period of V724 And

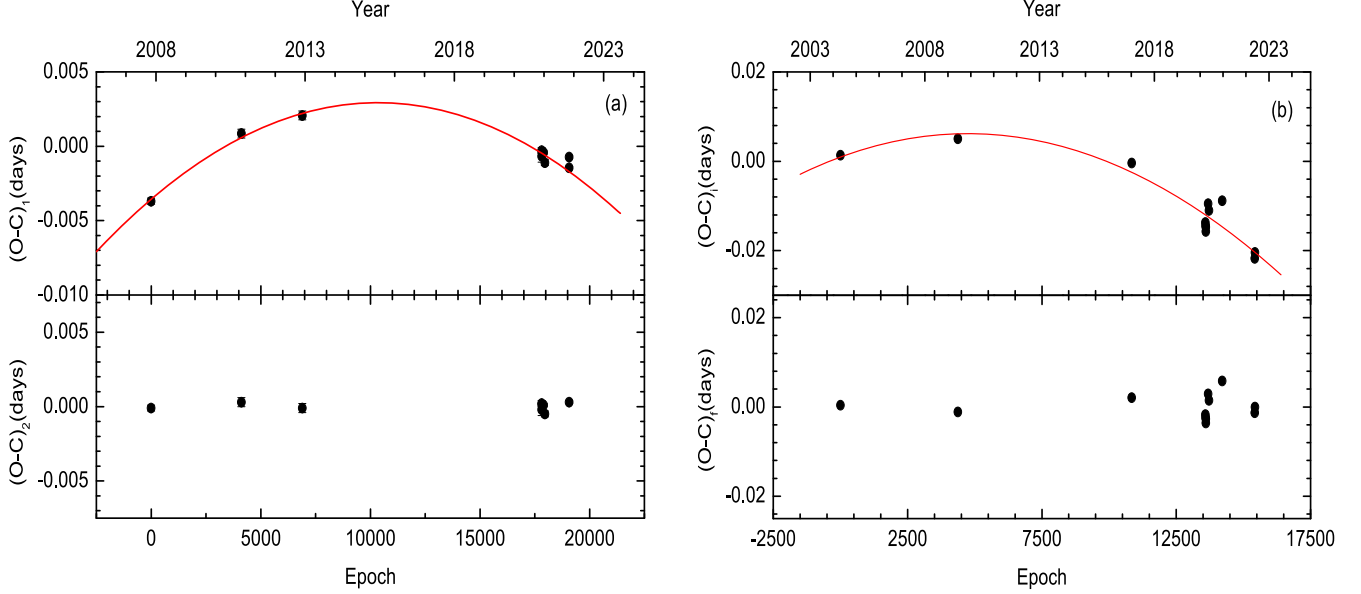


**Figure 7.** The  $(O-C)$  diagrams for V724 And (a) and QR Com (b). The continuous lines represent the period increasing of Equations (3) and (5), respectively.

may be decreasing. By using a linear least-squares method, we obtained the following quadratic ephemeris,

$$\begin{aligned} \text{Min.I} &= \text{HJD } 245408.6722(6) + 0.26817728(1) \\ &\times E - 6.09(6) \times 10^{-11} \times E^2 \end{aligned} \quad (3)$$

We calculated the final residuals of  $(O-C)_f$ , which are shown in the lower panel of Figure 7(a). From the coefficient of quadratic term of Equation (3), we easily computed a continuous period decrease rate of  $dP/dt = -1.66(\pm 0.02) \times 10^{-7}$  d/yr.

#### 4.2. QR Com

From the  $o-c$  gateway, the orbital period of QR Com is  $P = 0.427869$  days. Three light minimum times from TESS data are derived from the photometric solutions for TESS<sub>1933</sub>, TESS<sub>1937</sub> and TESS<sub>1940</sub>, which have been transferred from BJD to HJD. Based on our collected 12 light minimum times (see Table 7), the linear ephemeris was refined as follows,

$$\text{Min.I} = \text{HJD } 2453120.4564(39) + 0.42786751(39) \times E \quad (4)$$

Then we calculated the initial residuals  $(O-C)_i$ , which are displayed in the upper panel of Figure 7(b). From this figure, there exists a secular period decreasing. Therefore, the residuals of  $(O-C)_i$  were fitted by the following equation,

$$\begin{aligned} \text{Min.I} &= \text{HJD } 2453120.4502(4) + 0.42787120(2) \\ &\times E - 2.33(13) \times 10^{-10} \times E^2 \end{aligned} \quad (5)$$

We obtained the final residuals  $(O-C)_f$ , which are displayed in the lower panel of Figure 7(b). The orbital period of

QR Com may decrease with a rate of  $dP/dt = -3.98(\pm 0.17) \times 10^{-7}$  d/yr.

## 5. Discussions

### 5.1. Absolute Parameters and Evolutionary Status

According to the spectral types of  $G7/8$  for V724 And and  $F5/6$  for QR Com, their masses of the more massive are estimated at  $M_2 = 0.85(\pm 0.03) M_\odot$  and  $M_1 = 1.36(\pm 0.04) M_\odot$  (Cox 2000), respectively. With help of photometric solutions (i.e., LC<sub>2020</sub> for V724 And and LC<sub>2022</sub> for QR Com) and Kepler's third law of  $(M_1 + M_2) = 0.0134 \times a^3/P^2$ , we can obtain the separation between both components,  $a$ . Their luminosities were computed by a relation of  $L/L_\odot = (R/R_\odot)^2 (T/T_\odot)^4$ . All absolute physical parameters are listed at the end of Table 3.

In order to study the evolutionary states, we plotted both components in the mass–luminosity diagram of Figure 8, where black open and filled circles represent the less and more massive components for 406 contact binaries (Latković et al. 2021). The primaries lie on or above the ZAMS line, indicating that they are slightly evolved main-sequence stars. Meanwhile, the secondaries are located above the TAMS lines. The over-luminosities may be attributed to energy transfer (Zhang et al. 2020; Yang et al. 2022).

### 5.2. Magnetic Activity

Late type stars usually accompany magnetic activity, i.e., spots, flares and chromosphere activity. The LC solutions to different observational times exhibit vast differences in spots

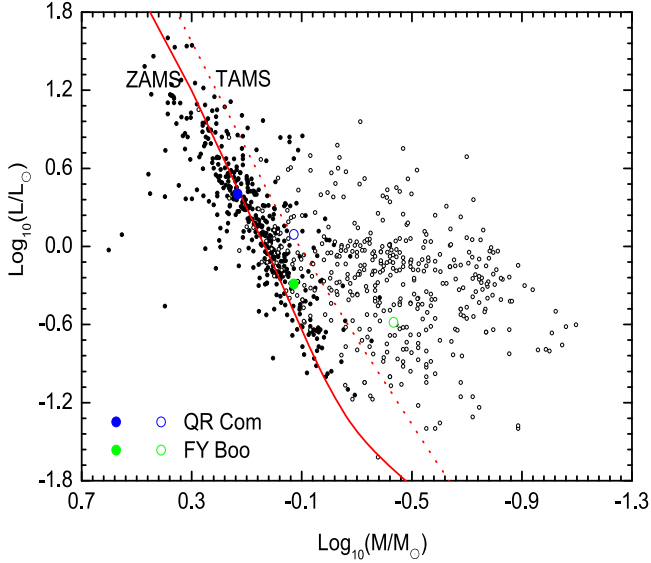


**Figure 8.** The evolutionary locations of both components for V724 And and QR Com in the H-R diagram. The filled and open symbols refer to the more massive component and the less one, respectively. The ZAMS and TAMS lines are constructed by the *BSE* code (Hurley et al. 2012).

longitudes for V724 And, i.e., spots longitude is  $77^{\circ}.2$  in LC<sub>2020</sub> solution, but it becomes  $285^{\circ}.3$  in LC<sub>2021</sub> solution. A similar behavior can be found in QR Com, spots longitude is  $103^{\circ}.1$  in TIC<sub>1933</sub> solution, but it becomes  $277^{\circ}.2$  in TIC<sub>1940</sub> solution. The spot variation may result in the LC changes of Figure 4(a).

H $\alpha$  emission line was considered as an indicator for chromosphere activity. However, chromosphere activity emission lines are influenced by photosphere absorption lines. Thus stars with similar surface effective temperatures and similar spectral types are usually selected to respect for the effect of photosphere, this is known as spectral subtraction techniques. From Figure 6, emission features of H $\alpha$  are clearly seen, this provides evidence for magnetic activity, and emission properties are from binary system because of low resolution of spectra. In the future, more photometric observations are needed to study the LC variations and high resolution spectra can help to study chromosphere activity.

### 5.3. Interpreting Period Decreasing

From Section 4, the orbital periods may be undergoing the secular period decreasing. Their period decrease rates are  $dP = -1.66(\pm 0.02) \times 10^{-7} \text{ day yr}^{-1}$  for V724 And and  $dP = -3.98(\pm 0.17) \times 10^{-7} \text{ day yr}^{-1}$  for QR Com, respectively. This situation occurs in several short-period contact binaries, such as EICVn (Yang 2011), IUCnc (Yuan et al. 2019), V1007 Cas (Li et al. 2018), BN Ari (Alton et al. 2018) and IOCnc (Liao et al. 2021). For contact binaries, the period decrease may be attributed the mass transfer from the less massive component to the more massive one, accompanied by mass and angular

momentum inevitably losing from the centering binary systems, which can be seen from Equation (9) of Yang et al. (2013). Due to the little contribution of the latter, we only consider the conserved mass transfer. The mass transfer rate from the secondary to the primary can be computed by the following equation (Singh & Chaubey 1986),

$$\frac{\dot{P}}{P} = \frac{3(1-q)\dot{M}_p}{qM_p}, \quad (6)$$

in which  $q$  is  $M_s/M_p$ . The subscripts of “ $p$ ” and “ $s$ ” refer to the primary and secondary components, respectively. We computed the mass transfer rates of  $dM_p/dt = -1.34(\pm 0.01) \times 10^{-7} M_{\odot} \text{ yr}^{-1}$  for V724 And, and  $dM_p/dt = -6.99(\pm 0.03) \times 10^{-7} M_{\odot} \text{ yr}^{-1}$  for QR Com, respectively. With mass transferring, the inner and outer critical Roche lobes will shrink, which causes the fill-out factor to increase. Therefore, the shallow-contact binaries, V724 And and QR Com, will evolve into deep-contact configurations. In the future, more high-precision light minimum times and radial velocities for two binaries will be obtained to identify our results.

### Acknowledgments

This research work is partly supported by the National Natural Science Foundation of China (No. 11873003), and the Open Project Program of the Key Laboratory of Optical Astronomy of NAOC. New photometry for V724 And and QR Com was performed by the 60 cm telescope at XLs of NAOC and the 84 cm telescope at the National Astronomical Observatory of Mexico.

### ORCID iDs

Raúl Meichel  <https://orcid.org/0000-0003-1263-808X>  
 Huiyu Yuan  <https://orcid.org/0000-0002-8018-3112>  
 Yuanguai Yang  <https://orcid.org/0000-0002-0151-6557>

### References

- Alton, K. B., Nelson, R. H., & Boyd, D. R. S. 2018, *AcA*, **68**, 159  
 Chen, X.-D., Wang, S., Deng, L., et al. 2020, *ApJS*, **249**, 18  
 Cox, A. N. 2000, in *Allen’s Astrophysical Quantities*, ed. A. N. Cox (4th edn.; New York: AIP Press)  
 Diethelm, R. 2013, *IBVS*, **6042**, 1  
 Diethelm, R. 2011, *IBVS*, **5760**, 1  
 Drake, A. J., Graham, M. J., Djorgovski, S. G., et al. 2014, *ApJS*, **213**, 9  
 Gaia Collaboration, Brown, A. G. A., Vallenari, A., et al. 2018, *A&A*, **616**, 1  
 Gazeas, K. D., Loukaidou, G. A., Niarchos, P. G., et al. 2021, *MNRAS*, **502**, 2879  
 Huang, L.-C., Ip, W.-H., Lin, C.-L., et al. 2020, *ApJ*, **892**, 58  
 Huang, Y., Liu, X.-W., Chen, B.-Q., et al. 2018, *AJ*, **156**, 90  
 Hurley, J. R., Tout, C. A., & Pols, O. R. 2012, *MNRAS*, **328**, 897  
 Kiraga, M. 2012, *AcA*, **62**, 67  
 Kwee, K. K., & van Woerden, H. 1956, *Bull. Astron. Ins. Nerth*, **12**, 137  
 Latković, O., Čeki, A., & Lazarević, S. 2021, *ApJS*, **254**, 10  
 Li, K., Xia, Q.-Q., Hu, S.-M., et al. 2018, *PASP*, **130**, id074201  
 Liao, W.-P., Li, L.-J., Zhou, X., et al. 2021, *RAA*, **21**, 041  
 Lienhard, P. 2021, *BAV*, **52**, 9  
 Liyun, Z., Zhongzhong, Z., Qiang, Y., et al. 2021, *MNRAS*, **491**, 6065

- Loukaidou, G. A., Gazeas, K. D., Palafouta, S., et al. 2022, *MNRAS*, 514, 5528
- Lucy, L. B. 1967, *Z. Astrophys.*, 65, 89
- Lucy, L. B. 1968, *ApJ*, 151, 1123
- O'Connell, D. J. K. 1951, *MNRAS*, 111, 642
- Paschke, A. 2009, *OEJV*, 116, 1
- Paschke, A. 2020, *BAV*, 40, 4
- Paschke, A. 2021, *BAV*, 55, 3
- Pi, Q.-F., Zhang, L.-Y., Bi, S.-L., et al. 2019, *ApJ*, 877, 75
- Pribulla, D. C., Chochol, P. A., Heckert, P. A., et al. 2001, *A&A*, 371, 997
- Qian, S.-B., He, J.-J., Zhang, J., et al. 2017, *RAA*, 17, 87
- Qian, S.-B., Wang, J.-J., Zhu, L.-Y., et al. 2014, *ApJS*, 212, 4
- Rucinski, S. M. 1973, *AcA*, 23, 79
- Samus, N. N., Kazarovets, E. V., Durlevich, O. V., et al. 2017, *Astron. Rep.*, 61, 80
- Singh, M., & Chaubey, U. S. 1986, *Ap&SS*, 124, 389
- Soderblom, D. R., Stauffer, J. R., Hudon, J. D., & Jones, B. F. 1993, *ApJS*, 85, 315
- Stępień, K. 2011, *AcA*, 61, 139
- Van Hamme, W. 1993, *AJ*, 106, 2096
- Webbink, R. F. 2003, *ASPC*, 293, 76
- Whelan, D. G., Chojnowski, S. D., Labadie-Bartz, J., et al. 2021, *AJ*, 167, 67
- Wilson, R. E., & Devinney, E. J. 1971, *ApJ*, 166, 605
- Wilson, R. E., & Van Hamme, W. 2014, *ApJ*, 780, 151
- Yang, Y., Yuan, H., Wang, S., & Dai, H. 2022, *AJ*, 163, 250
- Yang, Y.-G. 2011, *RAA*, 11, 181
- Yang, Y.-G., Qian, S.-B., & Dai, H.-F. 2013, *AJ*, 145, 60
- Yuan, H.-Y., Dai, H. F., & Yang, Y. G. 2019, *RAA*, 19, 85
- Zhang, X.-D., Qian, S.-B., & Liao, W.-P. 2020, *MNRAS*, 492, 4112
- Zhu, Z.-Z., Zhang, L.-Y., Meng, G., et al. 2021, *RAA*, 21, 84
- Zichgraf, F.-J., Engels, D., Hagen, H.-J., et al. 2003, *A&A*, 406, 535